

Impurity rotations in quantum versus classical solids: O₂ in solid hydrogens

Z. Li and V. A. Apkarian

Department of Chemistry, University of California, Irvine, California 92697-2025

(Received 4 December 1996; accepted 24 April 1997)

Molecular dynamics simulations based on pseudopotentials are used to characterize the difference between impurity rotations in classical versus quantum solids. The method is first applied to the pure solids and demonstrated to faithfully reproduce static and dynamical properties, in the form of pair distributions and phonon density of states of solid H₂(D₂). Then the rotations of molecular oxygen in the ground $X(^3\Sigma_g^-)$ and electronically excited state $A'(^3\Delta_u)$ is investigated. Where the substitutional impurity is small, O₂(X), in the classical solid, the cavity remains nearly spherical and the molecule undergoes rotation-translation coupled motion. In contrast, in the quantum solid, the lattice locally distorts around the impurity and forces librations with occasional reorientational hops as rotation-distortion coupled motion. These effects are amplified in the excited O₂(A') state, in which due to the larger molecular bond length, the angular anisotropy of the guest-host interaction is larger. Now, in the classical solid a small cage distortion forces the molecule into large amplitude librations. The molecule, however, reorients occasionally, when the lattice fluctuations lead to a nearly spherical cage geometry. In the quantum host, O₂(A') becomes a strict liblator, due to a large and permanent deformation of the soft cage. The results are used to rationalize experimental observations. © 1997 American Institute of Physics. [S0021-9606(97)02229-0]

I. INTRODUCTION

The spectroscopy of impurities isolated in quantum hosts,¹⁻¹² in solid hydrogen,¹⁻³ in hydrogen clusters,⁵ in solid and superfluid He,⁶⁻⁸ and in large He clusters⁹⁻¹² is an active field of research at present. One of the motivations of these studies is the fact that the impurity spectroscopy provides a molecular probe of the host, the peculiarities of which arise from the dominance of zero-point effects in these weakly interacting, light mass, media. That impurity rotations provide a useful handle for interrogating host properties on a molecular level, has been best illustrated by the recent high resolution spectroscopic studies of SF₆ entrapped in large superfluid He droplets.¹⁰

In an elegant experimental execution, high resolution spectra of SF₆ isolated in superfluid He droplets has been obtained. The spectra could be fit with an effective moment of inertia 30% that of the free molecule, leading to a possible interpretation that the rotor is a tight cluster of eight He atoms attached to the faces of the SF₆ octahedron.¹⁰ This picture would imply that due to the strong impurity host interactions, the first shell of atoms are radially localized as a classical solid, while the rest of the droplet acts as a frictionless superfluid on the atomic scale. Hindered rotors can also be treated in terms of effective moments of inertia that arise from the drag experienced by the rotor in a cage, or due to the cage pseudorotation.¹³ This could provide an alternate interpretation of the observed spectrum. Indeed, the radial distribution functions obtained in simulations of SF₆ trapped in He clusters show a larger frozen core, containing 22-23 He atoms.¹⁴

It is instructive to contrast the concept of a hindered rotor in a quantum host with that of free rotors in classical hosts. The most direct analysis of impurity rotations in clas-

sical hosts was recently provided in studies of CN radicals isolated in rare gas solids.¹⁵ It was shown, that even in the case of solid Xe, and despite the strong CN-Xe pair interaction, the radical freely rotates as evidenced from the fact that the spectroscopic moment of inertia is nearly identical to that of the bare radical. In essence, due to the preservation of the high symmetry of a substitutional cavity in the classical lattice, the angular anisotropy of the pair interaction is nearly completely lifted. This contention is directly demonstrated, by showing that upon destroying the cage symmetry in mixed rare gas solids, the CN ceases to rotate.¹⁵

Indeed, we expect a significant difference between classical and quantum cavities. In the first case, the integrity of a substitutional site containing a small impurity is expected to be preserved, since the structure of the solid is determined by potential energy, and collapse is prevented by the lateral potential repulsion among constituents of the cage. In contrast, in quantum solids where the structure is determined by both kinetic and potential parts of the Hamiltonian, the cavity is dynamic and would be expected to conform to the impurity. This consideration would lead us to the expectation that impurities that may be free rotors in a classical solid, may become strongly hindered in quantum solids since now rotation can only occur with full correlation with the surrounding cage motion, in effect a polaronic trapping of rotations. These expectations are verified in the model simulations which we present, which are parametrized to represent the rotations of O₂ in *o*-D₂ or *p*-H₂.

The choice of the system to be modeled here is motivated by our own experiments.³ The spectroscopy of O₂ isolated in solid hydrogens was studied experimentally via the formally nonallowed $A' \leftarrow X$ transition. The transition becomes allowed only in fcc sites where the molecule is ori-

ented along the [111] axis.⁴ This occurs only for a small fraction of the molecules, and then mainly in D₂, presumably because the main site of isolation in H₂ is locked in the hcp structure. The fluorescence is polarized, implying that at least in the excited state the molecule does not rotate. A librational progression is observed, with a librational frequency of 15 cm⁻¹ in the excited state. A Franck–Condon analysis of the progression intensities indicates that the molecular axis tips during the transition, that the angular minima in the ground and excited states are shifted. Beside the general issue of contrasting soft and hard lattices, the simulations reported below were designed to provide rationales for these experimental observations.

The simulations are based on a rather approximate method: classical simulations using pseudopotentials, constructed by Gaussian convolution of pair potentials. In the present, the pseudopotentials are constructed variationally, designed to be consistent with the structure and phonon density of states of the neat solid. A more primitive version of this method, pseudopotentials constructed based on structure only, we introduced earlier.¹⁶ There, we recognized that while useful, the pseudopotential had to be corrected to reproduce the exact position correlations in terms of $g(r)$. This correction seemed to be *ad hoc*, discouraging further development. We have since recognized that the correction can be made variationally, using in addition to $g(r)$ the phonon density of states as reference. It is with this approach that we interrogate the issue of classical-like versus quantumlike, stiff and soft lattices, and their effect on molecular rotations. Our approach finds formal justification in the method of centroid dynamics over pseudopotentials which has been rigorously developed by Voth and co-workers for treating the time dependent quantum Hamiltonian of systems of large dimensionality.^{17–19}

In what follows, in Sec. II, we outline the construct of the pseudopotentials and simulations of properties of the neat solid. In Sec. III we relate the results of simulations on O₂ doped hydrogen and deuterium, and close in Sec. IV with a discussion of implications.

II. CONSTRUCT OF PSEUDOPOTENTIALS

As an expedient approach to the dynamical simulations of quantum lattices, we previously proposed freezing the zero-point amplitude of the lattice points by convoluting them in the potential. Thus we define a pseudopotential

$$\tilde{V}_{ij}(\bar{r}) = \int_{-\infty}^{\infty} dr V_{ij}(r)G(r-\bar{r}) \quad (1)$$

which describes the interaction between a pair, i, j , in terms of the separation between the centers of Gaussians, \bar{r} , where

$$G(r-\bar{r}) = \frac{1}{2\sigma\sqrt{\pi}} \exp\left[-\frac{(r-\bar{r})^2}{4\sigma^2}\right] \quad (2)$$

is a Gaussian characterized by its width, σ . The width of the Gaussian is chosen to minimize the 0 K lattice sum of the pseudopotential

$$\frac{d\tilde{U}_{\text{tot}}}{d\bar{r}} = \frac{d}{d\bar{r}} \frac{1}{2} \sum_{ij} \tilde{V}_{ij}(\bar{r}) = 0 \quad (3)$$

in which i , and j extend over all pairs. Molecular dynamics simulations then track the motions of the \bar{r} centers of the Gaussians. From such a simulation, it is possible to obtain the pair distribution function of the centers, $g(\bar{r})$, directly, and the pair distribution function of lattice points, $g(r)$, may then be retrieved through a second Gaussian convolution¹⁶

$$g(r) = \int_{-\infty}^{\infty} d\bar{r} g(\bar{r})G(r-\bar{r}). \quad (4)$$

When σ is chosen with the criterion of Eq. (3), the computed $g(r)$ is more structured than the exact function obtained through quantum path integral Monte Carlo simulations.^{20,21} The exact $g(r)$ is retrieved by adjusting σ , by reducing it from the value determined by the minimization of Eq. (3).¹⁶ However, in the absence of a criterion other than the exact simulations, this approach did not seem very profitable. Yet, the essence of the fix is rather obvious. The above recipe for the choice of σ freezes the entire kinetic part of the Hamiltonian, in effect ballooning the particles into Gaussians. The structure is mostly determined by the static potentials—a classical lattice of hard Gaussians. The overlap between positions is then retrieved in part through the convolution in Eq. (4). However, this does not contain the proper kinetic correlations. Hereon, the Gaussian widths determined by the criterion of Eq. (3) will be designated by σ_c , with the implication that dynamics simulated by these pseudopotentials describes an effectively classical lattice of Gaussian particles.

Instead of the criterion of structure, we may choose σ variationally from a more dynamical measure, namely, by demanding that the proper phonon density of states of the lattice be reproduced. The phonon density of states of the neat lattice is obtained by diagonalization of the force matrix, \mathbf{K} , of second derivatives with respect to Cartesian coordinates of the centers

$$\mathbf{K}(\bar{r}, \sigma)_{lm} = \nabla_l \nabla_m U(\bar{r}, \sigma), \quad l, m = 1, \dots, 3N, \quad (5)$$

where l and m run over all coordinates of the lattice. σ is then varied, until the phonon density of states agrees with that previously calculated by self-consistent methods.²³ As it turns out, the Gaussian width chosen by this criterion, to which we will hereon refer as σ_q , also reproduces the proper $g(r)$.

Note, to the extent that the single particle functions can be assumed to be identical time independent Gaussians, the present formulation is the same as the prescription used in centroid dynamics over pseudopotentials.¹⁸ The assumption seems quite reasonable for systems near equilibrium, at temperature of a few K. The more refined treatment would be that of assuming that the particles are in locally quadratic effective potentials, therefore Gaussians, however, not restricted to have identical widths. We do not attempt a formal assessment of our approximation. Instead, we simply verify that equilibrium properties are obtained from dynamical cor-

TABLE I. Potential parameters.

Pseudopotentials	$C_{12}(\text{eV } \text{Å}^{12})$	$C_{10}(\text{eV } \text{Å}^{10})$	$C_8(\text{eV } \text{Å}^8)$	$C_6(\text{eV } \text{Å}^6)$
$\tilde{V}_c(\text{H}_2\text{-H}_2; \sigma=0.567)$	-30 530.7	9343.45	-607.055	1.539 39
$\tilde{V}_q(\text{H}_2\text{-H}_2; \sigma=0.43)$	-15 610.4	5255.52	-296.902	-5.541 35
$\tilde{V}_c(\text{D}_2\text{-D}_2; \sigma=0.42)$	-18 747.5	5959.72	-386.549	-2.103 24
$\tilde{V}_q(\text{D}_2\text{-D}_2; \sigma=0.21)$	-16 107.7	5095.28	-333.678	-2.680 54
$V(\text{O-D}_2)$	7074.94	-287.388	13.8675	-9.948 3
Morse potentials ^a for O ₂ :		$D_e(\text{eV})$	$\beta(\text{Å}^{-1})$	$r_e(\text{Å})$
O ₂ (X)		5.178	2.665	1.207
O ₂ (A')		0.868	3.335	1.530

^aFor the Morse form: $V=D_e[1-\exp(-\beta(r-r_e))]^2$.

relations, and fully recognize that our treatment is only an approximation, yet a useful one for providing insights into the problem at hand.

The pair distribution functions, $g(r)$, and the phonon density of states, $\rho(\omega)$, starting with the Silvera–Goldman pair potential for hydrogen,²² and using $\sigma_c=0.42$ a.u. and 0.567 a.u. for D₂ and H₂ were already reported.¹⁶ For the sake of simulations it is useful to have analytical forms for the pseudopotentials, \tilde{V} , which we fit to the expansion

$$\tilde{V}(\tilde{r}) = \frac{C_{12}}{\tilde{r}^{12}} + \frac{C_{10}}{\tilde{r}^{10}} + \frac{C_8}{\tilde{r}^8} + \frac{C_6}{\tilde{r}^6}. \quad (6)$$

These coefficients are given in Table I. The variationally obtained values of σ_q are 0.21 and 0.43 a.u. for D₂ and H₂, respectively. The coefficients of the \tilde{V}_q pseudopotentials obtained by this convolution of the Silvera–Goldman pair potential is also given in Table I. The simulated $g(r)$ for solid H₂, based on \tilde{V}_c and \tilde{V}_q , are shown in Fig. 1. The first of these yields a more structured $g(r)$ while the second yields the proper curve, one that agrees with the exact path integral quantum Monte Carlo simulations.²⁰ Henceforth, we will refer to all simulations based on \tilde{V}_c , as “classical,” while those based on \tilde{V}_q as “quantum.” The classical and

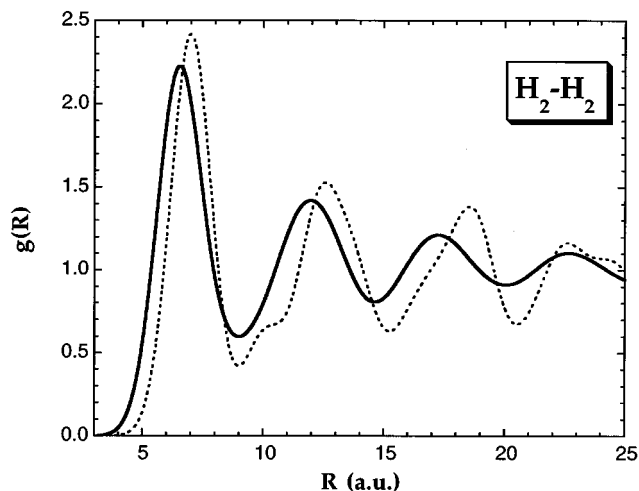


FIG. 1. Pair distribution function, $g(r)$ for solid hydrogen using pseudopotentials \tilde{V}_q (solid line) and \tilde{V}_c (dotted line).

quantum phonon density of states for H₂ and D₂ are given in Fig. 2. These are based on diagonalization of force matrices for cells containing 256 particles. The computed quantum $\rho(\omega)$, is in good agreement with that of Ref. 23 as far as the high frequency cutoffs and the Van Hove singularities are concerned. However, our distributions are coarse due to the limited number of modes considered.

Given the simultaneous reproduction of both structure and phonon density of states with a single pseudopotential, we proceed to simulations of the thermal rotations of an O₂ impurity in these solids, at ~ 4 K.

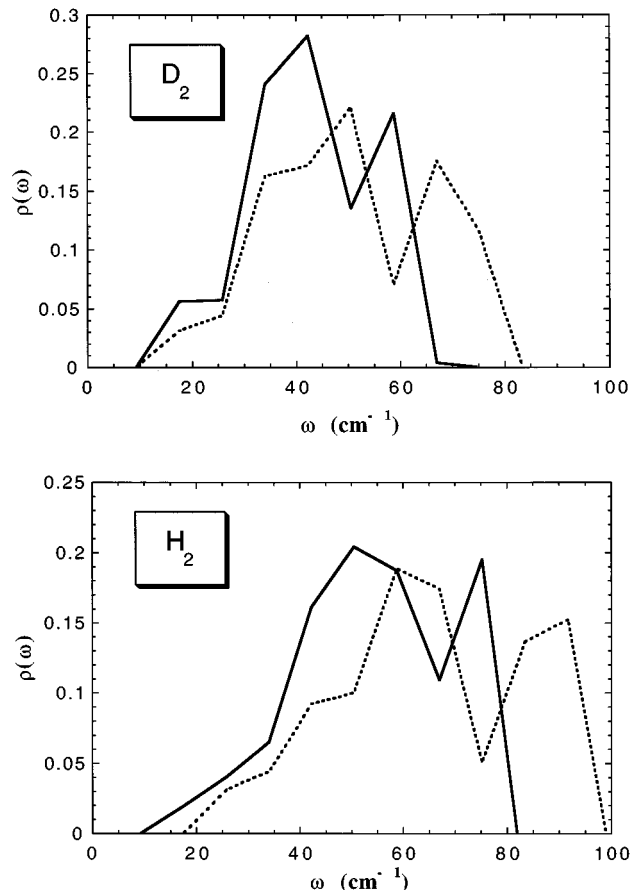


FIG. 2. Phonon density of states for solid H₂ and D₂ using pseudopotentials \tilde{V}_q (solid line) and \tilde{V}_c (dotted line).

III. SIMULATIONS

The pseudopotentials are used in a pairwise additive fashion in the classical molecular dynamics simulations of O₂ in the X and A' states, separately. All potential parameters used are summarized in Table I. An fcc cell of 500 particles, with periodic boundary conditions is used. O₂ is introduced substitutionally, by replacing it with one of the lattice points. Independent of initial orientation, the molecule always flips to point, on average, along the fourfold axis of the octahedral cage. The thermal motions of the system are then characterized through four measures:

(a) the time dependent orientation of the molecule:

$$\Omega(t) = \arccos[\mathbf{R}(t) \cdot \mathbf{R}(0)]; \quad (7)$$

(b) the instantaneous cage distortions from equilibrium, $D_{\alpha,\beta,\gamma}$, defined as the local lattice constant $D(t) = a(t) - a$; where a is the lattice constant of the perfect solid (or equivalently the distance between a - a planes), and α,β,γ correspond to the [100], [010], and [001], directions. For each direction there are four pairs of separations that can be computed among the 12 nearest neighbors to the impurity, and D is taken as the average of these four separations (see inset to Fig. 3);

(c) the principle moments of inertia of the cage, $I_{\alpha,b,c}$, obtained by diagonalization of the moment of inertia tensor, \mathbf{I} , with diagonal elements I_{xx}, I_{yy}, I_{zz} , given as

$$I_{xx} = \sum_{k=1}^{12} m(R_k^2 - X_k^2) \quad (8)$$

and off-diagonal elements, I_{xy}, I_{xz}, I_{yz} given as

$$I_{xy} = I_{yx} = - \sum_{k=1}^{12} mX_kY_k \quad (9)$$

in which the summation is limited to the nearest neighbors of O₂ and the vector positions of the cage atoms are measured from the O₂ center of mass $\mathbf{R}_k = \mathbf{r}_k - \mathbf{r}_{c.m.}$;

(d) the correlation between molecule and cage, in terms of the angle between principle moment of inertia and molecular axis

$$\phi = \arccos[\mathbf{I}_a(t) \cdot \mathbf{R}(t)]. \quad (10)$$

These time dependent measures of anisotropy, allow a full characterization of the dynamical correlations between cage and molecule, significantly more incisive than ensemble averaged statistical measures.

Note, since the O-D₂ potentials are assumed to be the same, independent of electronic excitation of the molecule, the main difference between simulations of the ground and excited states arises from the difference in the O₂ bond length: 1.2 Å in the X state, and 1.53 Å in the excited state. In each of these electronic states we carry out separate simulations using \tilde{V}_c and \tilde{V}_q pseudopotentials, referring to the first as classical and to the latter as quantum. The results of the simulations are collected in Figs. 3–6, to which we refer in the analyses given below.

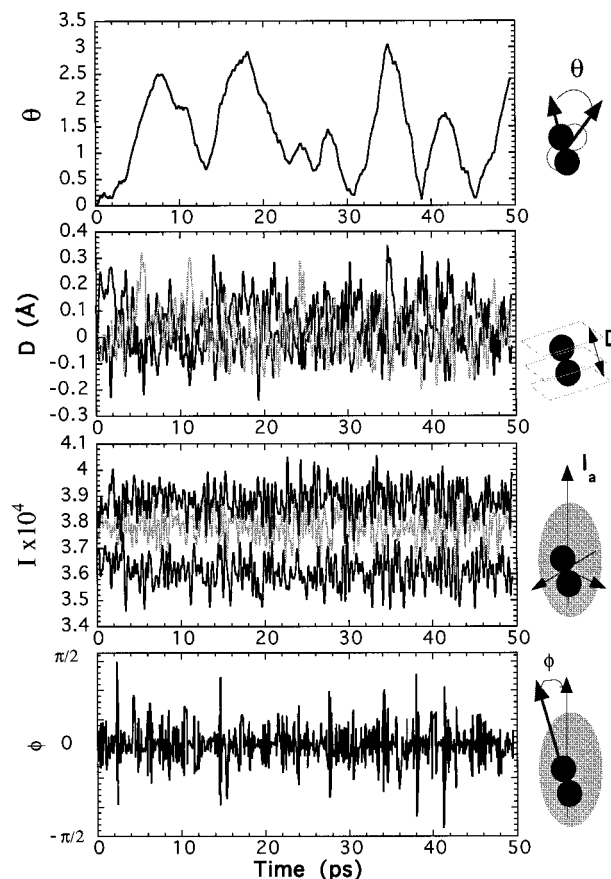
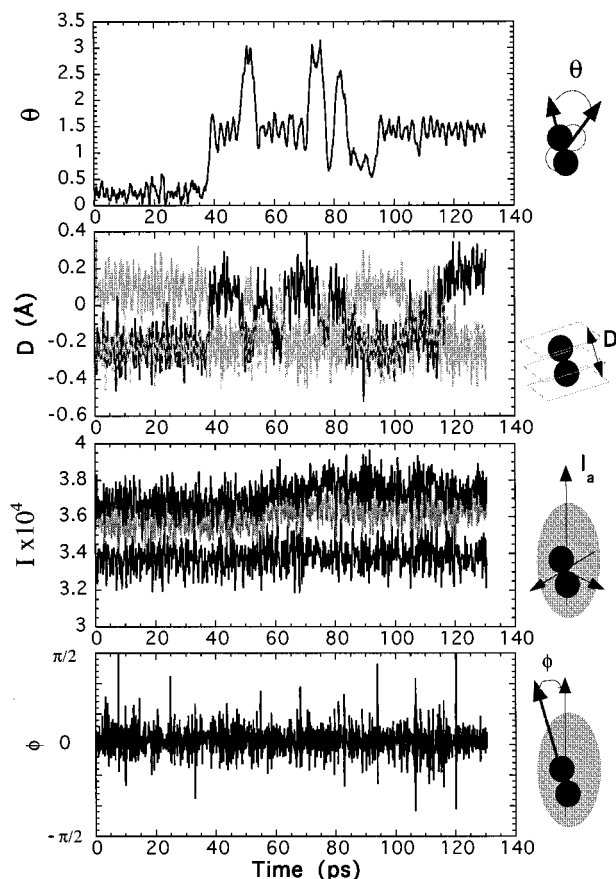


FIG. 3. O₂(X) in classical D₂, characterized by orientation, θ , cage distortions, $D_{\alpha,\beta,\gamma}$, cage moment of inertia as measured from the molecular center of mass, $I_{i,j,k}$, and the correlation between the principle cage moment of inertia and molecular orientation, ϕ . Note, for the sake of visibility, two components of D and I are shown in black while one in each is shown in gray.

A. O₂(X) in “classical” D₂

With reference to Fig. 3, it can be seen that in this case the molecular orientation, $\theta(t)$ fully spans the 0– π possible orientations. The cage does not distort as judged by the fact that on average $D_\alpha = D_\beta = D_\gamma \sim 0$, and their fluctuations fully overlap. Nevertheless, the molecule remains slightly eccentric in the undistorted cage, which leads to the small separation in the moments of inertia. The principle moment of inertia and the molecular orientation remain correlated: on average, $\phi = 0$, implying that the orientation and eccentricity are correlated. This is the picture of the rotation-translation-coupling (RTC) model for motion,²⁴ which has long been recognized as the principle mechanism for rotation of small molecules, such as diatomic hydrides, in substitutional sites of classical solids.²⁵ The separation between center of mass and center of interaction, which is measured by the splitting in I_i in the present gives rise to n, j combination bands in ir active molecules, where n is the translational quantum number (local phonon) and j is the free rotor quantum number.²⁴ A Fourier transform of $\theta(t)$, shown in Fig. 7(a) yields the classical rotational frequency, from which the effective moment of inertia can be extracted noting that classically:

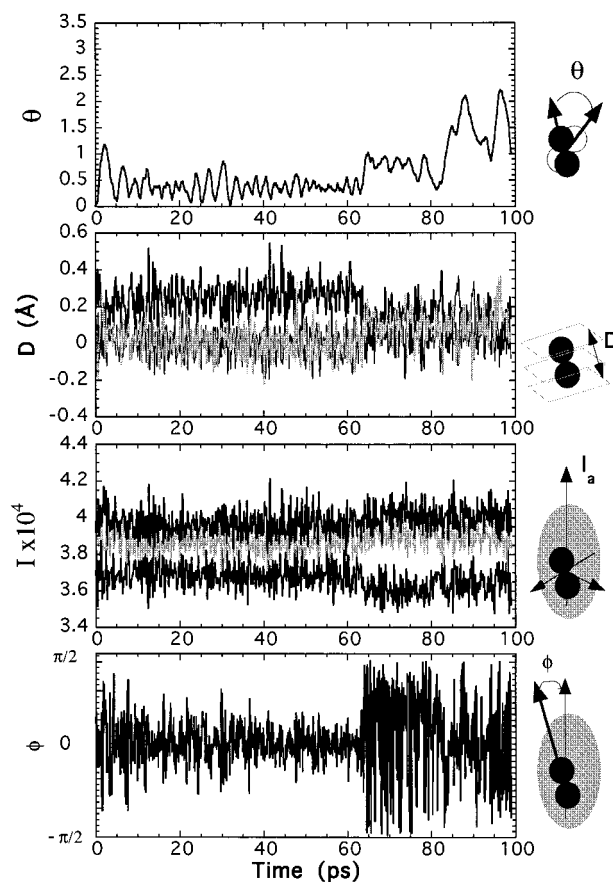
FIG. 4. O₂(X) in quantum D₂, same format as in Fig. 3.

$$\frac{1}{2}I\omega^2 = \frac{1}{2}k_B T. \quad (11)$$

From the observed frequency of 3.1 cm^{-1} , the simulation temperature of 4.5 K, a moment of inertia of $1.8 \times 10^{-39} \text{ g cm}^2$ is obtained, which, within the uncertainties of the simulation, should be regarded as the same as the moment of inertia of the free molecule, of $1.91 \times 10^{-39} \text{ g cm}^2$. Thus although the observed motion is described as rotation-translation coupling, the effect of this perturbation on the rotational frequency of the molecule is negligible (note, drag would raise the moment of inertia). In its ground state, in classical solid D₂, the C₂ impurity is essentially a free rotor.

B. O₂(X) in “quantum” D₂

The same simulation as above are now carried out using \tilde{V}_{q-} as the pseudopair potential. A very different picture emerges from the decomposition shown in Fig. 4. The molecule is no longer a free rotor, $\theta(t)$ oscillates with small amplitudes and makes occasional jumps of $\pi/2$, flipping between fourfold axes of the site. The cage has a uniaxial distortion, $D_\alpha > D_\beta = D_\gamma$. The distortion is dynamic and its orientation flips as judged by the crossings in D_i . Moreover, all of the molecular orientational jumps are accompanied with a change of orientation in the cage distortion axis. No crossings are observed in the principle moments of inertia, which implies that the eccentricity of the molecule adiabatically

FIG. 5. O₂(A') in classical D₂, same format as in Fig. 3.

follows the distortion. This picture is reinforced by the tight correlation observed between principle moment of inertia and molecular orientation: the rotational jumps observed in $\theta(t)$ produce no signature in $\phi(t)$. We therefore have a picture of a libror in a locally distorted cage, which undergoes orientational hops carrying along with it the cage distortion. The distortion of the cage in the quantum solid, Fig. 4, should be contrasted with the nearly spherical cavity in the classical solid, Fig. 3. In the softer solid, the cage conforms to the to molecular potential anisotropy.

C. O₂(A') in “classical” D₂

O₂(A'), due to its larger bond length, can no longer freely rotate in the classical host, as observed by $\theta(t)$ in Fig. 5. The molecule undergoes large amplitude librations during the first 60 ps of the simulation, during which time the cage is slightly distorted, stretched along the molecular axis. Near 60 ps, the molecular orientation hops, oscillates along the new equilibrium direction, and then rotates. This motion occurs when the cage assumes a nearly spherical geometry, when $D_\alpha = D_\beta = D_\gamma$. The collapse of the cage distortion, and the reorientation of the molecule, is accompanied by anisotropy in the moment of inertia tensor: As in the ground state classical simulation, the rotation occurs in the undistorted cage but with a separation between centers of mass and center of interaction, and the eccentricity remains correlated

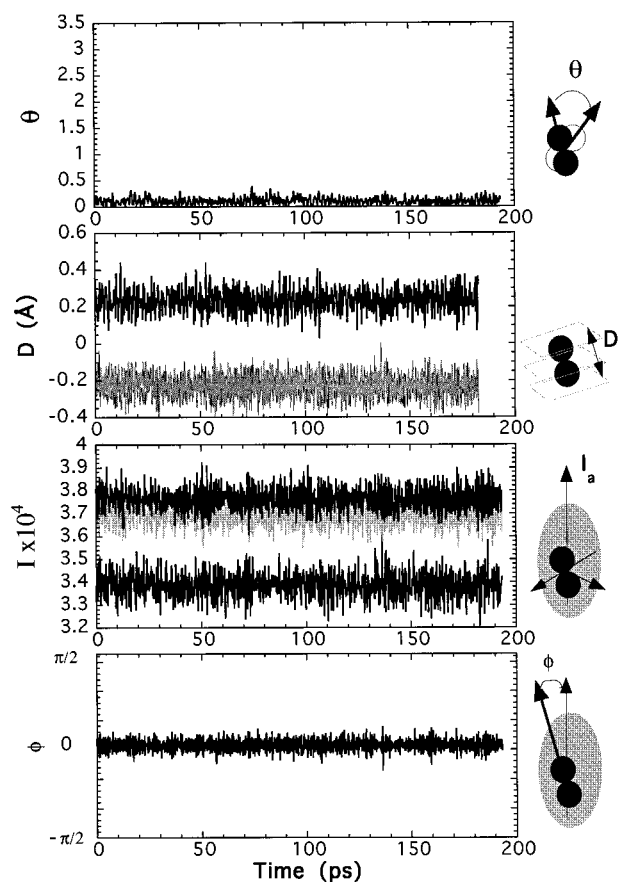


FIG. 6. O₂(A') in quantum D₂, same format as in Fig. 3.

with the molecular orientation. The picture is then one of orientational locking due to cage distortions, and reorientation induced by the dynamical collapse in cage distortion.

D. O₂(A') in "quantum" D₂

In the softer quantum lattice, the larger angular anisotropy of the elongated molecule in the A' state is sufficient to permanently distort the cage, forcing a strictly librational motion on the molecule, see Fig. 6. The cage is elongated along the molecular axis, and is compressed around its waist. Fourier transform of $\theta(t)$, see Fig. 7(b), now yields a librational frequency of 15 cm⁻¹, same as the librational frequency observed experimentally.³ This close agreement should be regarded as fortuitous, nevertheless, the effect of completely locked orientation is verified by the fully polarized fluorescence observed in the experiments.

E. Solid H₂

The same set of four simulations were repeated by changing the mass of the host atoms to that of H₂, and by adjusting the lattice constant of the simulation cell to that of solid H₂. The overall picture remains the same, except the effects observed in D₂ are somewhat more amplified in H₂. A few of the differences deserve comment. In all cases, librational amplitudes and cage distortions in solid H₂ are

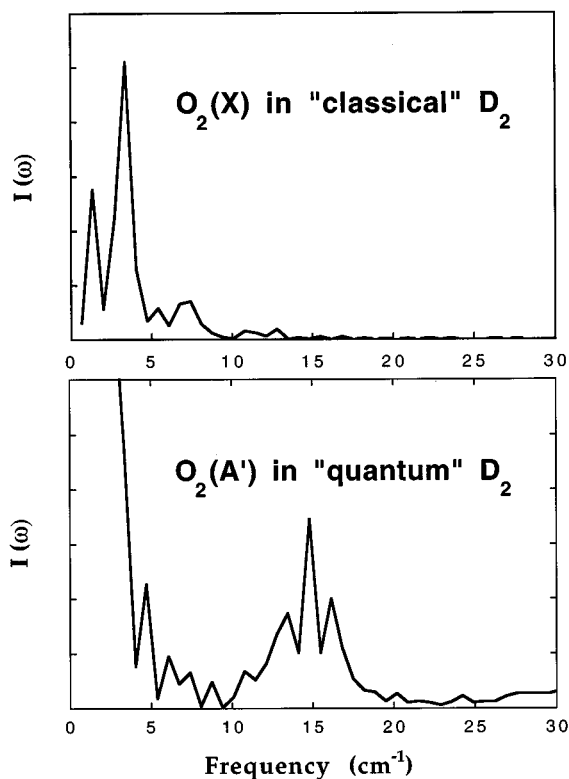


FIG. 7. Power spectra of molecular orientation, $\Theta(t)$. Top panel shows the rotational frequency of O₂(X) in a classical solid D₂, and corresponds to Fourier transformation of the time file shown in Fig. 3. Bottom panel shows the librational frequency of O₂(A') in a quantum solid D₂, derived from the time file shown in Fig. 6.

larger than in D₂. However, the differences in frequencies are within the widths of the peak width in the power spectra, i.e., indistinguishable. An interesting observation relates to the difference in cage distortions. In the case of quantum solid D₂, the cage distorts by stretching along the molecular axis ($D_\alpha = 0.2$ Å for O₂(A') in Fig. 6) while compressing along the molecular belt ($D_\beta = D_\gamma = -0.2$ Å in Fig. 6). The stretch is obviously the result of repulsion between O and lattice atoms, and accordingly the compression may be construed to be the result of crowding. Given the larger lattice constant of H₂, in the case of the A' state $D_\alpha = 0.2$ Å while $D_\beta = D_\gamma = -0.4$ Å, is observed, i.e., the radial distortion is nearly doubled, while the axial distortion is the same. More notable is the case of the X state in the quantum H₂, where now there is no extension of the cage along the molecular axis, while the radial cage compression remains as -0.4 Å. Therefore, in this case, it is safe to conclude that the very large radial cage compression is strictly the result of attractive forces between guest and host. In short, the very soft H₂ lattice may distort around the impurity either due to attractive or repulsive interactions. A cage that conforms to the impurity potential is a valid picture to have for these quantum hosts.

IV. CONCLUDING REMARKS

We have presented approximate simulations of extended systems dominated by quantum zero-point motions, through

the use of pseudopotentials that are variationally derived to reproduce properties of the system. While by design the method is approximate, it is already useful in developing insights regarding dynamics in quantum hosts. In addition to the treatment of impurity rotations executed here, we have also used the same approach in calculations of reactive dynamics in solid hydrogens.²⁶ While we have not provided formal justification for the method, our approach closely parallels the method of centroid dynamics over pseudopotentials advanced by Voth *et al.*¹⁷⁻¹⁹

The simulations reported in this work help validate a picture of an easily deformable lattice for quantum hosts to be contrasted with classical hosts. While the exact magnitudes of these distortions will depend on the particular choice of a guest and host, the general trend remains. As a result, in solid hydrogens, and for non spherical guests, rotations are expected to be quenched into coupled molecule-cage oscillations. This picture may not entirely hold for He, and in particular for superfluid He. There, the guest along with a shell of atoms may still rotate, as is suspected for the case of SF₆.⁹

Despite the approximate nature of these simulations, surprisingly good is the agreement with the relatively limited experimental observations on this system. The model explains the absence of rotation of O₂(A'), in solid D₂ and H₂, which is verified by the observation of polarized laser induced fluorescence over this transition.³ Moreover, the predicted librational frequency of 15 cm⁻¹ in O₂(A') is in excellent agreement with the librational progression observed there. Further, the present simulations provide a rationale for the absence of observable fluorescence in undistorted H₂ and the presence of a librational progression in solid D₂. As discussed in the experimental analysis, only O₂ molecules pointing in the [111] direction of the fcc lattice are optically active. The present simulations indicate that the preferred molecular orientation in the ground state is along [100] and strongly locked. As such, the large distortion of the H₂ lattice stabilizes the relative molecule-cage orientation, and prevents it from pointing along the [111] axis. In the case of D₂, the distortion is smaller, and in the ground state the molecule undergoes large amplitude oscillations. Thus Franck-Condon overlap can be achieved between the ground state [100] orientation and the excited state [111] orientation in the case of solid D₂, leading to a Franck-Condon progression as observed experimentally, and already identified as implying a change in molecular orientation during the electronic transition.

ACKNOWLEDGMENT

This research was made possible through an AFOSR University Research Initiative grant, F49620-1-0251.

- ¹M. E. Fajardo, S. Tam, T. L. Thompson, and M. E. Cordonnier, *Chem. Phys.* **189**, 351 (1994).
- ²T. Momose, M. Uchida, N. Sogoshi, M. Miki, S. Masuda, and T. Shida, *Chem. Phys. Lett.* **246**, 583 (1995); T. Momose, M. Miki, M. Uchida, T. Shimizu, I. Yoshizawa, and T. Shida, *J. Chem. Phys.* **103**, 1400 (1995).
- ³A. V. Danilychev, V. E. Bondybey, V. A. Apkarian, S. Tanaka, H. Kajihara, and S. Koda, *J. Chem. Phys.* **103**, 4292 (1995).
- ⁴The argument is based on recognizing that the transition becomes allowed by mixing $\Pi(L=2, \Lambda=\pm 1)$ character in the $\Delta(L'=2, \Lambda'=\pm 2)$ state, which requires a substitutional site in which the lowest order spherical harmonics that represent the full symmetry of the site, Y_{kl} , must obey $L+L' \geq l \geq |L-L'|$ and $z \rightarrow z'$ precluding odd $k-l$ values. In Ref. 3, the condition for the vector addition was miss stated as $l \geq L+L'$, however, the conclusion remains, since the lowest acceptable values of l for the substitutional site are 0, 4, 6...
- ⁵C. Callegari, J. Higgins, F. Stienkemeier, and G. Scoles, *Proceedings of HEDM Conference (Boulder, 1996)*; K. Kinugawa, P. B. Moore, and M. L. Klein, *J. Chem. Phys.* **106**, 1154 (1997).
- ⁶Q. Hui, J. L. Persson, J. H. M. Beijersbergen, and M. Takami, *Laser Chem.* **15**, 221 (1995).
- ⁷S. I. Kanorsky, M. Arndt, R. Dziewior, and A. Weis, *Phys. Rev. B* **49**, 3645 (1994).
- ⁸B. Tabbert, M. Beau, H. Gunther, W. Haubler, C. Honninger, K. Meyer, B. Plagemann, and G. zu Putlitz, *Z. Phys. B* **97**, 425 (1995).
- ⁹A. Scheidemann, B. Schilling, J. P. Toennies, and J. A. Northby, *Physica B* **165**, 135 (1990); R. Frochtenicht, J. P. Toennies, A. Vilesov, *Chem. Phys. Lett.* **229**, 1 (1994).
- ¹⁰M. Hartmann, R. E. Miller, J. P. Toennies, and A. Vilesov, *Phys. Rev. Lett.* **75**, 1566 (1995); *Science* **272**, 1631 (1996).
- ¹¹F. Stienkemeier, J. Higgins, W. E. Ernst, G. Scoles, *Z. Phys. B* **98**, 413 (1995); *Phys. Rev. Lett.* **74**, 3592 (1995); *J. Chem. Phys.* **102**, 615 (1995); S. Goyal, D. L. Schutt, and G. Scoles, *J. Phys. Chem.* **97**, 2236 (1993); S. Goyal, D. L. Schutt, G. Scoles, and G. N. Robinson, *Chem. Phys. Lett.* **196**, 123 (1992).
- ¹²B. E. Callicott, D. D. Mar, V. A. Apkarian, and K. C. Janda, *J. Chem. Phys.* **105**, 7872 (1996).
- ¹³J. Manz, *J. Am. Chem. Soc.* **102**, 1802 (1980).
- ¹⁴K. B. Whaley, *Int. Rev. Phys. Chem.* **13**, 41 (1994).
- ¹⁵G. Schallmoser, A. Thoma, B. E. Wurfel, and V. E. Bondybey, *Chem. Phys. Lett.* **219**, 101 (1994); B. E. Wurfel, N. Caspary, J. Agreiter, A. Thoma, A. M. Smith, and V. E. Bondybey, *J. Chem. Phys.* **92**, 351 (1995).
- ¹⁶M. Sterling, Z. Li, and V. A. Apkarian, *J. Chem. Phys.* **103**, 5679 (1995).
- ¹⁷J. Cao and G. A. Voth, *J. Chem. Phys.* **99**, 10070 (1993); **100**, 5106 (1994); **101**, 6157 (1994).
- ¹⁸J. A. Cao and G. A. Voth, *J. Chem. Phys.* **101**, 6168 (1994).
- ¹⁹M. Pavese and G. A. Voth, *Chem. Phys. Lett.* **249**, 231 (1996).
- ²⁰D. Scharf, G. J. Martyna, D. Li, G. A. Voth, and M. Klein, *J. Chem. Phys.* **99**, 9013 (1993); D. Scharf, G. J. Martyna, and M. Klein, *ibid.* **99**, 8997 (1993).
- ²¹D. Li and G. A. Voth, *J. Chem. Phys.* **96**, 5340 (1992).
- ²²I. F. Silvera and V. V. Goldman, *J. Chem. Phys.* **69**, 4209 (1978).
- ²³A. B. Anderson, J. C. Raich, and R. D. Etters, *Phys. Rev. B* **14**, 814 (1976).
- ²⁴H. Friedman and S. Kimel, *J. Chem. Phys.* **41**, 2552 (1964); **43**, 3925 (1965); **44**, 4359 (1966); **47**, 3589 (1967).
- ²⁵A. J. Barnes, in *Vibrational Spectroscopy of Trapped Species*, edited by H. E. Hallam (Wiley, New York, 1973), Chap. 4.
- ²⁶Z. Li, V. A. Apkarian, and L. B. Harding, *J. Chem. Phys.* **106**, 942 (1997).